Thermal Time Evolution of Non-Flaring Active Regions Determined by SDO/AIA

Paul J. Wright[1], Iain G. Hannah[1], Nicholeen M. Viall[2], Alec Mackinnon[1], Jack Ireland[2,3], Stephen J. Bradshaw[4]

[1]University of Glasgow, [2]NASA Goddard Space Flight Center (GSFC), [3]ADNET Systems Inc, [4]Rice Uniersity

e: paul.wright@glasgow.ac.uk

University of Glasgow

EPSRC Engineering and Physical Sciences Research Council

THE ROYAL SOCIETY

Summary

The cross-correlation of pixel-level *SDO*/AIA light curves (time-lag analysis: Viall & Klimchuck, 2011; 2012; 2013; 2015; 2016) is becoming an increasingly popular analysis technique in order to investigate coronal heating. While the observed time-lag between two *SDO*/AIA channels can be indicative of heating or cooling, the inherent multi-thermal nature of the *SDO*/AIA responses can mask the true dynamical situation of the underlying plasma (**Fig 3**).

We therefore recover the thermal time evolution at the pixel-level by producing Differential Emission Measure (DEM) maps (Hannah & Kontar, 2012, **GitHub***; Cheung et al., 2015), and present a proof of concept for time-lag analysis on DEM maps of the non-flaring active region presented in Viall & Klimchuk 2012, VK2012, **Figs 1, 5**.

We present both the *SDO*/AIA images (**Fig 1**) and recovered DEM maps (**Fig 5**) for one set of co-temporal observations presented in VK2012. We produce the light curves (**Figs 2, 6**) for a pixel over two hours of observations, both in the *SDO*/AIA channels (as in VK2012) and in different temperature bands derived from the DEM maps (calculated for each of these times; The data, and DEM for the pixel is shown at one time in **Figs 1, 4, 5**). The cross-correlation (CC) time-lag is determined in both *SDO*/AIA channels and temperature bands and recovers similar behaviour of brightenings that cool over time (**Figs 2, 6**).

... Overleaf we further describe our investigation of time-lag analysis for the whole map.

1. *SDO*/AIA Images

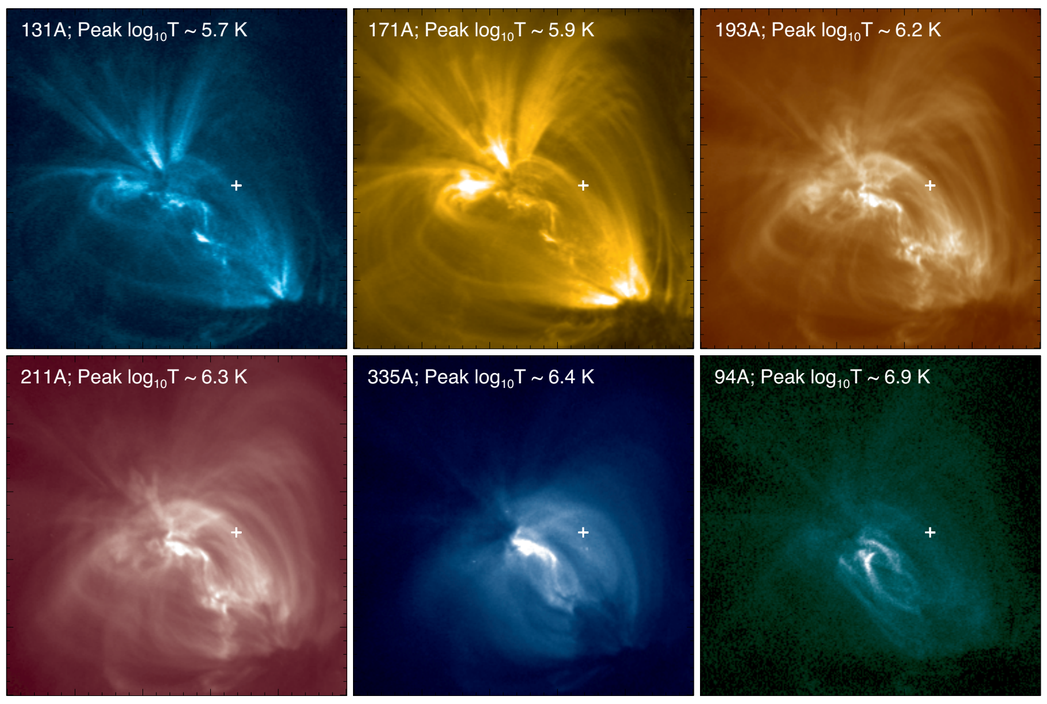

Figure 1: *SDO*/AIA Images in the six coronal filters at one time during the 12 hour observations of AR 11082 (~6000s; **Fig 2**), plot in order of increasing peak temperature response. A single pixel of interest used herein is plot as a white cross.

2a. DEMs

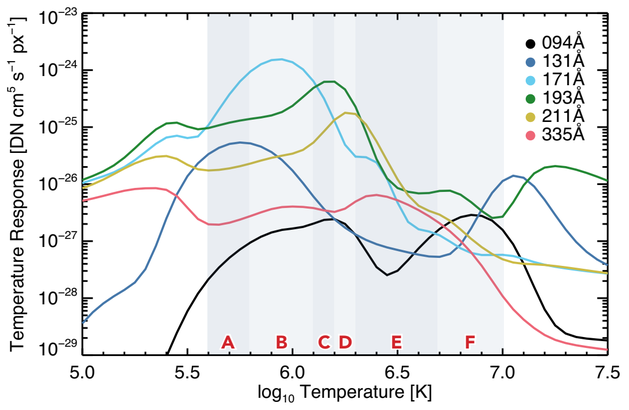

Figure 3: *SDO*/AIA Temperature response functions for the six coronal filters. Also highlighted are the temperature bins (alternating, dark and light blue bars, **A - F**, chosen to coincide with the peak temperatures of each channel) for DEM map analysis.

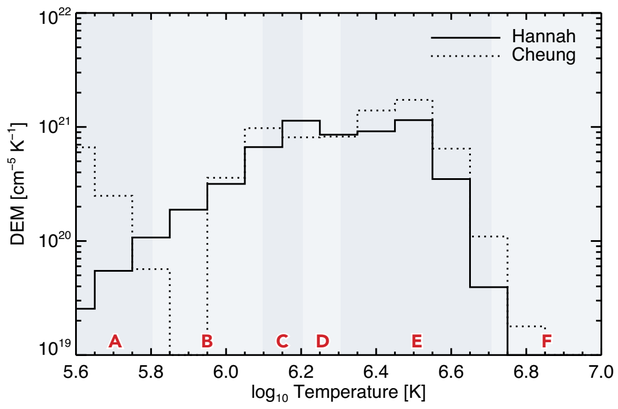

Figure 4: The DEM of the pixel highlighted in **Fig 1**, calculated at one time (~6000s; **Fig 2**) from Hannah et al, 2012 (and Cheung et al., 2015) *before* interpolation into bins **A - F** for analysis in **Figs 5, 6.**

2b. DEM Maps

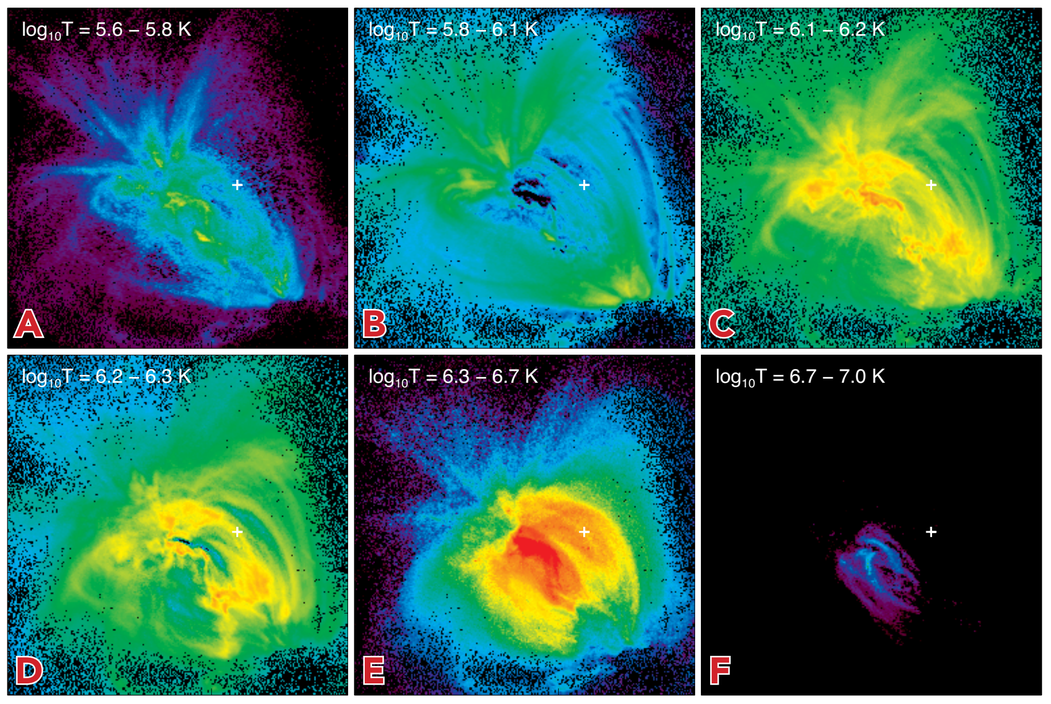

Figure 5: DEM Maps calculated at one time (~6000s; **Fig 2**), interpolated into six temperature bins (**A - F**) chosen to coincide with the peak temperatures of the SDO/AIA channels (**Figs 3, 4**), and are plot as maps of $\log_{10}$(DEM), over $\log_{10}$(DEM) = 19, 21, with the single pixel in **Figs 1, 2, 4,** highlighted as a white cross.

SDO/AIA (λ) Time-Lags

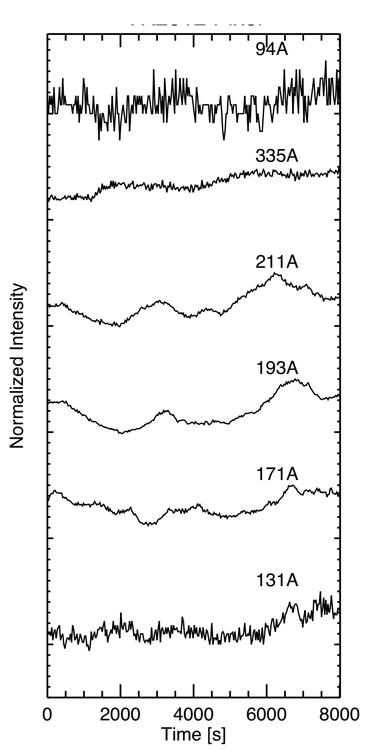

Figure 2: *Left:* Normalized, and systematically y-offset, *SDO*/AIA light curves for all six coronal channels for the chosen pixel in **Fig 1** for a 2 hour sample of the 12 hours of observation. *Bottom*: Time-Lag vs. Cross-Correlation values for select pairs of *SDO*/AIA light curves implying cooling. [As Figures 3,4 in VK2012].

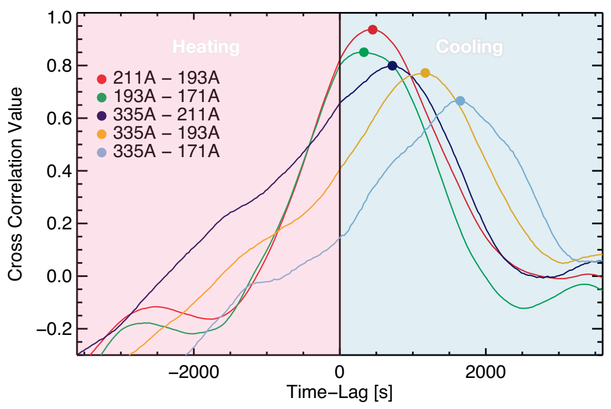

DEM (T) Time-Lags

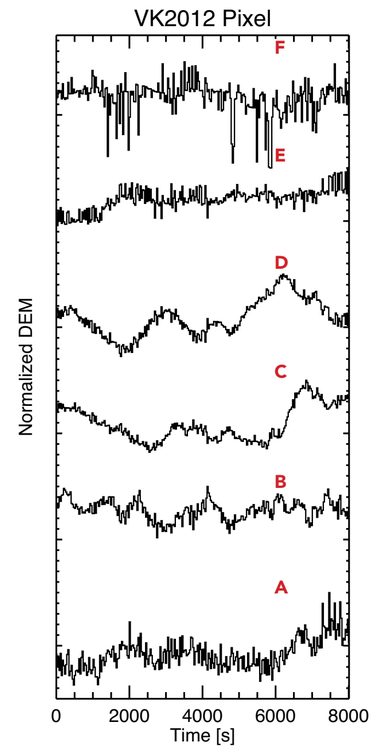

Figure 6: *Left:* Normalized, and systematically y-offset, DEM light curves of the pixel in **Figs 1, & 4**, and in each DEM map shown in **Fig 5** for a 2 hour sample of the 12 hours of observation. *Bottom*: Time-Lag vs. Cross-Correlation values for the cross correlation of the $\log_{10}$(DEM) light curves; the recovery of cooling similar to that in **Fig 4** is observed.

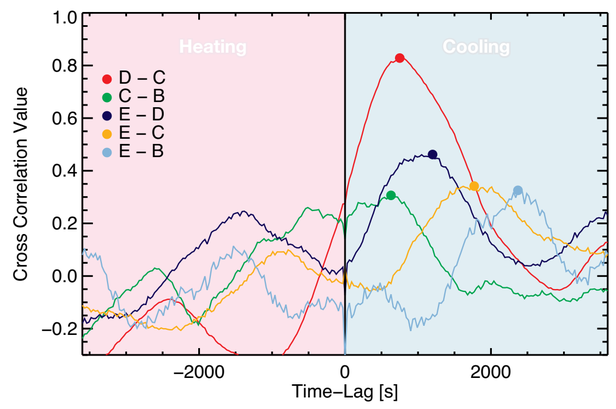

***Code available on GitHub at:**
http://github.com/ianan/demreg

References:
Cheung, M. C. M., et al 2015, ApJ, 807, 143; Dinkelaker, A. N., & MacKinnon, A. L., 2013, Sol Phys, 282, 471; Hannah, I. G., & Kontar, E. P., 2012, A&A, 539, A146; Ireland, J., et al. 2015, ApJ, 798, 1; Sakamoto, Y. et al. 2008, ApJ, 689, 1421; Terzo, S., et al. 2011, ApJ, 736, 111; Viall, N. M., & Klimchuk, J. A. 2011, ApJ, 783, 24; Viall, N. M., & Klimchuk, J. A. 2012, ApJ, 753, 35; Viall, N. M., & Klimchuk, J. A. 2013, ApJ, 771, 115; Viall, N. M., & Klimchuk, J. A. 2015, ApJ, 799, 58; Viall, N. M., & Klimchuk, J. A. 2015, ApJ, 799, 58

Thermal Time Evolution of Non-Flaring Active Regions Determined by SDO/AIA

Paul J. Wright[1], Iain G. Hannah[1], Nicholeen M. Viall[2], Alec Mackinnon[1], Jack Ireland[2,3], Stephen J. Bradshaw[4]

[1]University of Glasgow, [2]NASA Goddard Space Flight Center (GSFC), [3]ADNET Systems Inc, [4]Rice Uniersity

e: paul.wright@glasgow.ac.uk

University of Glasgow

EPSRC Engineering and Physical Sciences Research Council

THE ROYAL SOCIETY

Summary (cont.)

For 12 hours of AR 11082 observations (VK2012) we present the DEM time-lag map (DEM temperature bins **C** & **B**; **Fig 7 (top)**) in comparison to the *SDO*/AIA time-lag map for 193A & 171A (**Fig 7 (bottom)**; as in VK2012). We see that the DEM time-lag map displays the same general features observed in the *SDO*/AIA time-lag map with additional information concentrated within the AR core.

To understand the output DEM time-lag approach presented here we perform identical analysis on the output of EBTEL simulations (EBTEL returns the DEM that can be used to synthesize AIA data) for the same set of channels as in **Fig 7**. These EBTEL simulations are described in detail in Viall & Klimchuk 2013, but consist of 1000 impulsively heated EBTEL simulations (for AR 11082) along the line of sight, and return both coronal and transition region (TR) DEMs over time; the recovered DEMs and *SDO*/AIA data can then be compared to the output of the EBTEL simulations.

Figs 8a, 9a show the EBTEL DEM and *SDO*/AIA variability (temperature bins **C** & **B**; channels 193A & 171A [see **Fig 4**]) against the equivalent, recovered data from DEM analysis, for the coronal (**§ 4a**) and TR (**§ 4b**) simulations over a 350 min window; **Figs 8b, 9b** show the respective time-lags. The EBTEL, and recovered time-lags, match well with the CC values peaking at near-identical time-lags; there is an observed time-lag shift in CC-peak between the *SDO*/AIA and DEM time-lags for the coronal simulations, but not for the TR ones. This confirms that TR plasma would still register as zero time-lag. **Fig 10** confirms that steady light curves (averaged fluxes + Poisson noise) would produce no substantial time-lag signature.

Our next step is to extensively investigate the time-lag analysis for other pairs of channels, and different parts of the AR. Obtaining these light curves in the different temperature bands also gives us the opportunity to apply a variety of techniques, in addition to time-lag analysis, to investigate the heating and cooling such as: Fourier Power Spectra Analysis (Ireland et al., 2015); Intermittency (Dinkelaker & MacKinnon, 2013); and Asymmetry (Sakamoto et al., 2008; Terzo et al., 2011).

3. Time-Lag Maps

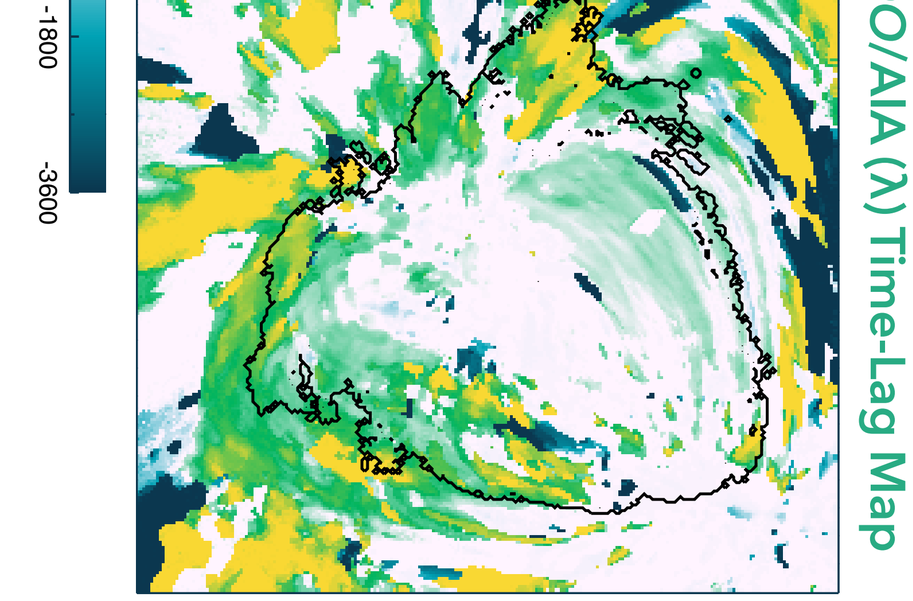

Figure 7: Time-Lag maps for DEM Temperature bins (top; **C - B**), with a black contour enclosing the pixels in which the DEM was successfully recovered for each time-step). *Bottom*: Time-lag maps for the *SDO*/AIA channels (193A - 171A, c.f. VK2012). The black contour indicates the equivalent location of the DEM Time-lag map (top). The DEM time-lag map displays similar time-lags, with additional information recovered in the AR core.

4a. EBTEL: Corona

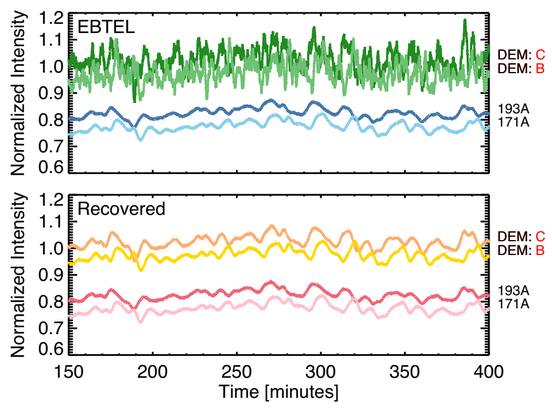

Figure 8a: Normalized, and systematically y-offset light-curves for selected DEM bins (**C** & **B**) and *SDO*/AIA channels (193A & 171A) obtained from EBTEL simulations (top) and DEM recovery (bottom).

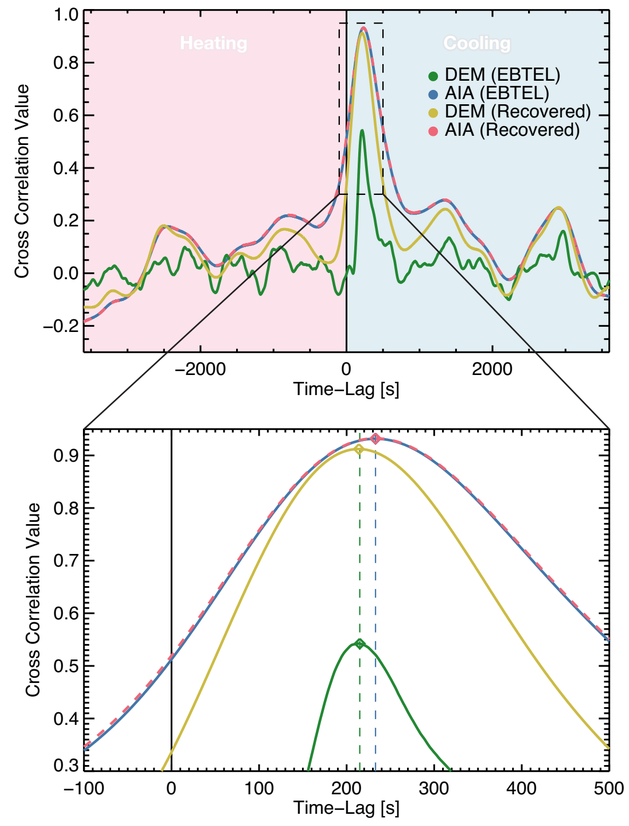

Figure 8b: Time-Lag vs. CC value for the CC of the *SDO*/AIA, and DEM light curves (**Fig 8a**). The recovered *SDO*/AIA and DEM time-lags peak at CC values that agree with those obtained from EBTEL simulations.

We note that the CC peaks of the DEM time-lags are shifted with respect to the CC peaks in the *SDO*/AIA time-lags (bottom; vertical dashed lines indicate peak time-lags for EBTEL DEMs, and *SDO*/AIA time-lags); all four CC peaks are highlighted with diamonds.

4b. EBTEL: Transition Region

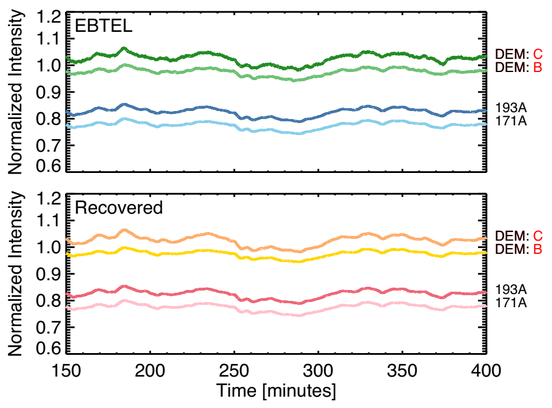

Figure 9a: Normalized, and systematically y-offset light-curves for selected DEM bins (**C** & **B**) and *SDO*/AIA channels (193A & 171A) obtained from EBTEL simulations (top) and DEM recovery (bottom).

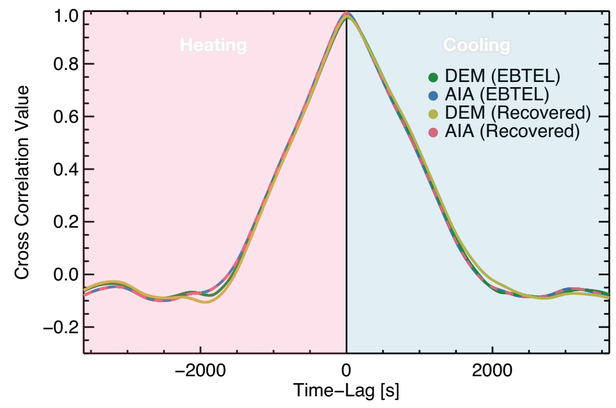

Figure 9b: Time-Lag vs. CC values for the CC of the *SDO*/AIA, and light curves (**Fig 9a**). The recovered *SDO*/AIA and DEM time-lags agree with the EBTEL simulations with zero time-lags.

4c. Steady Light Curves

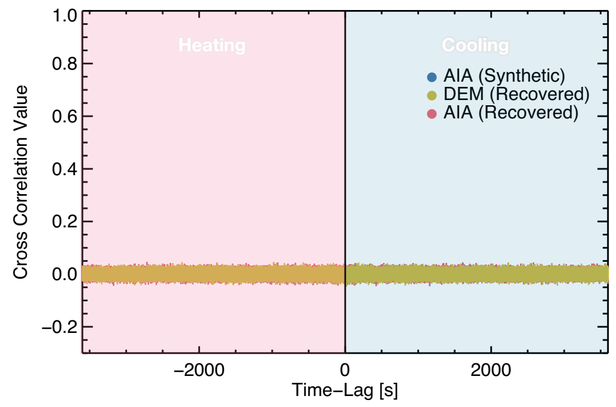

Figure 10: Time-Lag vs. CC values for the CC of synthetic *SDO*/AIA data (synthesized from a set of representitive diffuse emission fluxes + Poisson noise) against the recovered *SDO*/AIA and DEM time-lags.

***Code available on GitHub at:**
http://github.com/ianan/demreg

References:
Cheung, M. C. M., et al 2015, ApJ, 807, 143; Dinkelaker, A. N., & MacKinnon, A. L., 2013, Sol Phys, 282, 471; Hannah, I. G., & Kontar, E. P., 2012, A&A, 539, A146; Ireland, J., et al. 2015, ApJ, 798, 1; Sakamoto, Y. et al. 2008, ApJ, 689, 1421; Terzo, S., et al. 2011, ApJ, 736, 111; Viall, N. M., & Klimchuk, J. A. 2011, ApJ, 783, 24; Viall, N. M., & Klimchuk, J. A. 2012, ApJ, 753, 35; Viall, N. M., & Klimchuk, J. A. 2013, ApJ, 771, 115; Viall, N. M., & Klimchuk, J. A. 2015, ApJ, 799, 58; Viall, N. M., & Klimchuk, J. A. 2015, ApJ, 799, 58